*Inflammatory Bowel Diseases*, 2022, **28**, 1143–1150
https://doi.org/10.1093/ibd/izac046
Advance access publication 23 March 2022
**Leading Off**

# Mechanoscopy: A Novel Device and Procedure for *in vivo* Detection of Chronic Colitis in Mice

**Shijie He, PhD,[*,†,‡,§,#] Dara A. Azar, PhD,[*,†,‡,§,#] Farid Nasr Esfahani, MD,[*,†,‡,§] Golara A. Azar, BS,[¶] Tarek Shazly, PhD,[‖] and Nima Saeidi, PhD[*,†,‡,§,]**

From the *Division of Gastrointestinal and Oncologic Surgery, Department of Surgery, Massachusetts General Hospital, Boston, MA, USA
†Center for Engineering in Medicine and Surgery, Department of Surgery, Massachusetts General Hospital, Boston, MA, USA
‡Shriners Hospital for Children, Boston, MA, USA
§Harvard Medical School, Boston, MA, USA
¶Department of Electrical Engineering and Computer Sciences, University of California Los Angeles, Los Angeles, CA, USA
‖Department of Mechanical Engineering, University of South Carolina, Columbia, SC, USA

#These authors contributed equally.
Address correspondence to: Nima Saeidi, 51 Blossom St., Room 207, Boston, MA, 02114, USA (nsaeidi@mgh.harvard.edu).

**Background:** Gut stiffening caused by fibrosis plays a critical role in the progression of inflammatory bowel disease (IBD) and colon cancer. Previous studies have characterized the biomechanical response of healthy and pathological gut, with most measurements obtained *ex vivo*.

**Methods:** Here, we developed a device and accompanying procedure for *in vivo* quantification of gut stiffness, termed *mechanoscopy*. Mechanoscopy includes a flexible balloon catheter, pressure sensor, syringe pump, and control system. The control system activates the balloon catheter and performs automated measurements of the gut stress-strain biomechanical response.

**Results:** A gut stiffness index (GSI) is identified based on the slope of the obtained stress-strain response. Using a colitis mouse model, we demonstrated that GSI positively correlates with the extent of gut fibrosis, the severity of mucosal damage, and the infiltration of immune cells. Furthermore, a critical strain value is suggested, and GSI efficiently detects pathological gut fibrotic stiffening when the strain exceeds this value.

**Conclusions:** Based on these results, we envision that mechanoscopy and GSI will facilitate the clinical diagnosis of IBD.

## Lay Summary

Here, we present a novel procedure/device, termed *mechanoscopy*, which we have demonstrated to accurately detect and differentiate between fibrosis and inflammation in rodent models of colitis. Thus, *mechanoscopy* offers a translationally relevant approach for ultrasensitive and minimally invasive IBD diagnosis.

**Key Words:** gut fibrosis; tissue stiffness; gut inflammation

## INTRODUCTION

Gut stiffening caused by fibrosis is a hallmark of inflammatory bowel disease (IBD) and colon cancer.[1–3] Previous studies have established gut stiffening as a causative factor for the most severe manifestations of IBD and intestinal strictures.[2,4,5] Moreover, stiffening is also reported to facilitate cancer metastasis.[6,7]

Different strategies and devices have been invented and applied to measure gut stiffness under pathological conditions.[1,2,4,5,8] For instance, both an indentation system[1] and a MicroElastometer[4] have been used to determine the stiffness of excised healthy and fibrotic human gut samples *ex vivo*. Furthermore, Stidham et al, utilizing the ultrasound elasticity imaging method, demonstrated a 4-fold increase in the elastic modulus of fibrotic stenotic intestine in IBD patients ($0.96 \pm 0.25$ kPa in healthy intestine compared with $4.14 \pm 1.88$ kPa in fibrotic intestine).[8] Although these studies demonstrate the translational value of gut stiffness for diagnosing IBD, the methods used to quantify gut stiffness in these studies are primarily conducive to *ex vivo* measurements or lack adequate resolution, both of which limit their translational potential. In the present work, we developed mechanoscopy for the high-resolution quantification of gut stiffness *in vivo*.

Mechanoscopy enables the acquisition of *in vivo* stress-strain curves of the gut in a colitis murine model. Ulcerative colitis (UC) and Crohn's disease (CD) are the commonest types of IBD. We defined the gut stiffness index (GSI) based on the local slope of the stress-strain curves and efficiently applied it to predict gut fibrosis and IBD severity in mice. These results support mechanoscopy as a promising avenue for the translational application of gut stiffness measurement in IBD diagnosis.

## METHODS

### Mechanoscopy Setup (in vivo and ex vivo)

As constructed, the mechanoscope can be modified for either *in vivo* (Figure 1A) or *ex vivo* testing. Under both *in vivo* and *ex vivo* modalities, the mechanoscope setup encompasses

Received for publication: November 19, 2021. Editorial Decision: February 10, 2022

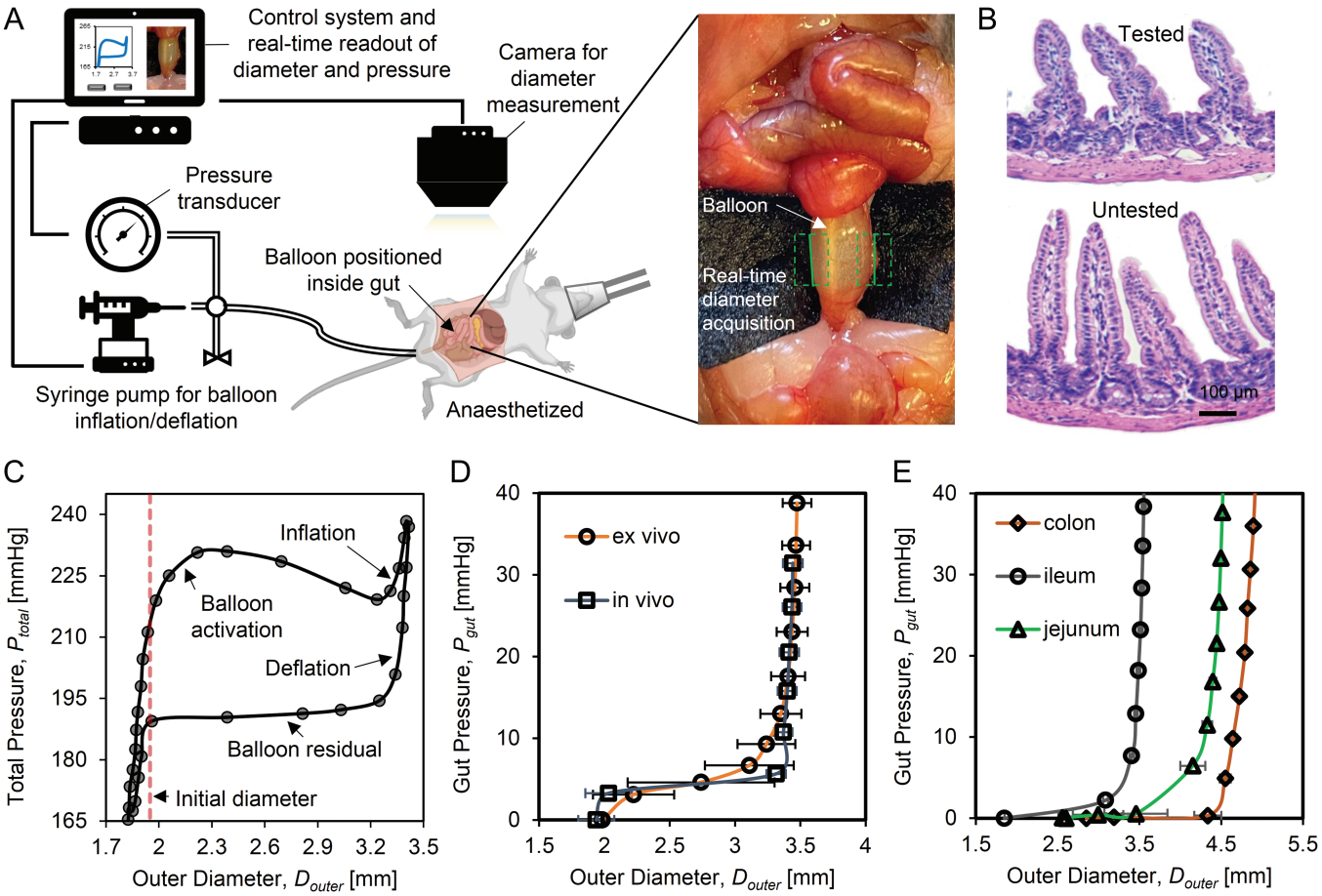


**Figure 1.** Schematic of real-time gut diameter and stiffness measurement using mechanoscope. A, The mechanoscope includes control system, pressure transducer, balloon catheter, syringe pump for the balloon inflation/deflation, and gut diameter measurement camera. The control system coordinates the pressure transducer and gut diameter measurement camera to automatically record real-time pressure and diameter. The gut diameter measurement module is integrated into the control system, which identifies the gut (green dashed box) and detects the gut edges (green solid line). B, H&E staining shows that during testing, no damage of mucosa and muscle layer occurs in tested samples compared with an adjacent untested section of ileum. C, In testing cycles the gut outer diameter, $D_{outer}$ is recorded in correspondence with total pressure, $P_{total}$. A test cycle includes 4 phases, balloon activation, inflation, deflation, and balloon residual. The initial diameter (red dashed line) marks the gut diameter at rest prior to testing. D, Gut pressure ($P_{gut}$) is calculated after removing balloon residual from $P_{total}$. No significant differences are detected for $P_{gut}$-$D_{outer}$ tissue response under *in vivo* and *ex vivo* testing conditions. E, $P_{gut}$ as a function of $D_{outer}$ are measured from different gut segmentations, jejunum, ileum, and colon samples.

the following key components: LabVIEW-based control system equipped with a gut diameter measurement module, pressure transducer, water-filled balloon catheter, and syringe pump for actuating balloon inflation/deflation. For a typical *in vivo* mechanoscopy test, the deflated balloon catheter is situated inside the gut lumen by surgery. During testing, the mice are anesthetized using isoflurane as an anesthetic agent according to Institutional Animal Care and Use Committee (IACUC) guidelines. After placing the mice in supine position, the abdomen is accessed via a U-shaped incision. For *in vivo* studies of the jejunum and ileum, small vertical incisions are made for catheter placement 2 mm above the positions selected for the *ex vivo* studies. For *in vivo* studies of the colon, the balloon catheter was guided through the anus and placed at the required positions (proximal, mid, or distal). In the *ex vivo* setup, 12 mm specimens were dissected from the middle of the colon, proximal jejunum (30 mm after the ligament of Treitz), and distal ileum (5 mm above the cecum), respectively, and flushed with 37°C phosphate-buffered saline (PBS). The dissected specimens were mounted in the bioreactor with a closed flow system based on oxygenated PBS to ensure intestinal tissue viability during testing.[9]

The gut diameter measurement module was customized and embedded in the software of the control system to ensure correct registration of pressure ($P$) and gut outer diameter ($D_{outer}$) for each measurement. For the gut diameter measurement, digital images of the gut at the test sites were automatically sequenced and recorded on camera. Any warp or distortion of the camera lens was corrected by means of standard dot grid calibration. The gut diameter measurement module in the control system used a series of digital images acquired during testing to identify the gut, detect the gut edges, and then automatically calculate the gut outer diameter ($D_{outer}$).

To facilitate gut diameter measurement, a black cloth was placed under the section of interest to create the highest contrast background (Figure 1A). Using the control system, the balloon was inflated at a rate of 0.5 mL/min under quasistatic loading while the gut outer diameter and balloon pressure were actively measured. The balloon pressure was recorded at a frequency of 1.9 Hz. During the inflation phase, the balloon contacted the gut

lumen and inflated the gut to a predefined maximum radial stretch. We estimated the maximum physiological circumferential stretch of the gut by measuring changes in gut diameter during chyme digestion (2 ± 0.25, 2.2 ± 0.16, and 2.1 ± 0.15 for jejunum, ileum and colon, respectively) to ensure that the imposed radial stretch remained within physiological range. Initial gut diameter data were acquired from the average of several real time camera detections before balloon inflation.

For *ex vivo* analysis, the sample was housed in a bioreactor equipped with a PBS-based perfusion/bathing system and a temperature sensor. The *ex vivo* balloon inflation/deflation measurement was identical to that of the previously described but performed in the bioreactor with perfused PBS at 37°C. With both the *ex vivo* and *in vivo* measurements, five cycles of inflation-deflation preconditioning up to 60% of the maximum radial strain were performed to minimize the viscus response and variability of the soft tissue.[10–13] Following the preconditioning cycles, three inflation-deflation cycles were completed and collected during each test for further analysis. After the *in vivo* tests, we repeated the measurements with the *ex vivo* setup to confirm that the measurements from the *in vivo* setup and the *ex vivo* setup were in accordance with each other. The animals fully recovered after mechanoscopy and behaved normally.

## Software for Data Analysis

We developed the mechanoscopy software, which is based on a database of 480 tests, to automatically analyze the obtained pressure-diameter curves. All information on software for data analysis is available in the supplemental materials. The algorithm consists of (1) preprocessing, (2) stress-strain calculation, and (3) postprocessing. In the preprocessing phase, following an initialization, any unrealistic data entry caused by sensor noise is removed via a thresholding operation. The upper bound of the deflation curves is extracted by detecting the farthest point. In the software, this data point is identified as the one at the greatest Euclidean distance from the origin (0,0) in the total pressure ($P_{total}$)-outer diameter ($D_{outer}$) plot. The gut pressure ($P_{gut}$) was calculated by,

$$P_{gut}=P_{total}-Z \tag{1}$$

where $Z$ is the residual pressure of balloon calculated based on the initial intersecting outer diameter and a linear fit of the plateau region of the deflation curve. To ensure systematic averaging across multiple iterations, gut pressure ($P_{gut}$) values are defined based on groupings within a width of 5 mmHg. Mean circumferential stress and mean circumferential strain are then calculated for each measured pressure-diameter data point as

$$Circumferential\ Stress\ \sigma=\frac{P_{gut}\ D_{inner}}{D_{outer}\ -\ D_{inner}} \tag{2}$$

$$Circumferential\ Strain\ \ \varepsilon=\frac{D_{inner}}{D_{\ outer,\ 0}-2\ t} \tag{3}$$

where $D_{outer,0}$ and $t$ are, respectively, the initial undeformed diameter and the undeformed wall thickness. $D_{inner}$ is the deformed inner diameter calculated based on the assumption of incompressibility.[14,15]

$$D_{inner}=2\times\sqrt{\left(\frac{D_{outer}}{2}\right)^2-\left(\frac{D_{outer,\ 0}}{2}\right)^2+\left(\frac{D_{outer,\ \ 0}}{2}-t\right)^2} \tag{4}$$

To quantify the gut biomechanical response from the postprocessing results, the local slope of the stress-strain curve was defined as the gut stiffness index (GSI). Interpolation between measured data points was performed using the Gaussian Kernel Regression model. Then, using a linear regressor in the "neighborhood" of a given strain, the GSI was calculated. The neighborhood radius is a hyperparameter that can be modified by the user, and here it was set to a default value of 1.

## Mice

A total of 40 25-30-g 10-week-old male C57BL/6J male mice were procured (The Jackson Laboratory, Bar Harbor, ME). The animals were housed and maintained on a 12-hour light/dark cycle with access to food and water ad libitum. All experimental procedures were approved by the Institutional Animal Care and Use Committee (IACUC) of the Massachusetts General Hospital and met the guidelines of National Institutes of Health (NIH). The mice were divided into 4 groups comprising 2 disease models (acute colitis and chronic colitis) and a control group for each.

## DSS-induced Colitis

The colitis murine model was developed by introducing dextran sulfate sodium (DSS) in drinking water over a controlled regimen and duration.[16–18] Acute colitis was developed by administering 3% (wt/vol) DSS (molecular weight 36-50 kDa, MP Biomedicals, Irvine, CA) in drinking water for 7 consecutive days (Figure 2A).[19] To induce chronic colitis, DSS was administered 1 week followed by normal water for 2 weeks for a total of 3 cycles (Figure 2A).[17,19] Control groups included age- and sex-matched animals that were only given normal water. Animals were observed daily for body weight, water/food consumption, stool consistency, and presence of blood in feces and around the anus. The animals showed signs of inflammation (eg, body weight loss, blood in stools, and piloerection) approximately 5 days after the initiation of DSS administration, which fully resolved by the end of the first recovery week.

## Histology

After the mechanoscope measurement, tissue samples from the jejunum, ileum, and colon collected from the tested/untested site were fixed in 10% formalin and further processed for histological studies. Following sectioning at 5-μm thickness, prepared sections were deparaffinized and then stained with hematoxylin and eosin (H&E), Masson's trichrome, and the DAPI-TRITC combination for collagen IV staining.[20–23] Image J was used to calculate the fibrosis score and immunefluorescent intensity.

## Calculation of Correlation Coefficient

The correlation coefficient was calculated based on the correlation function,

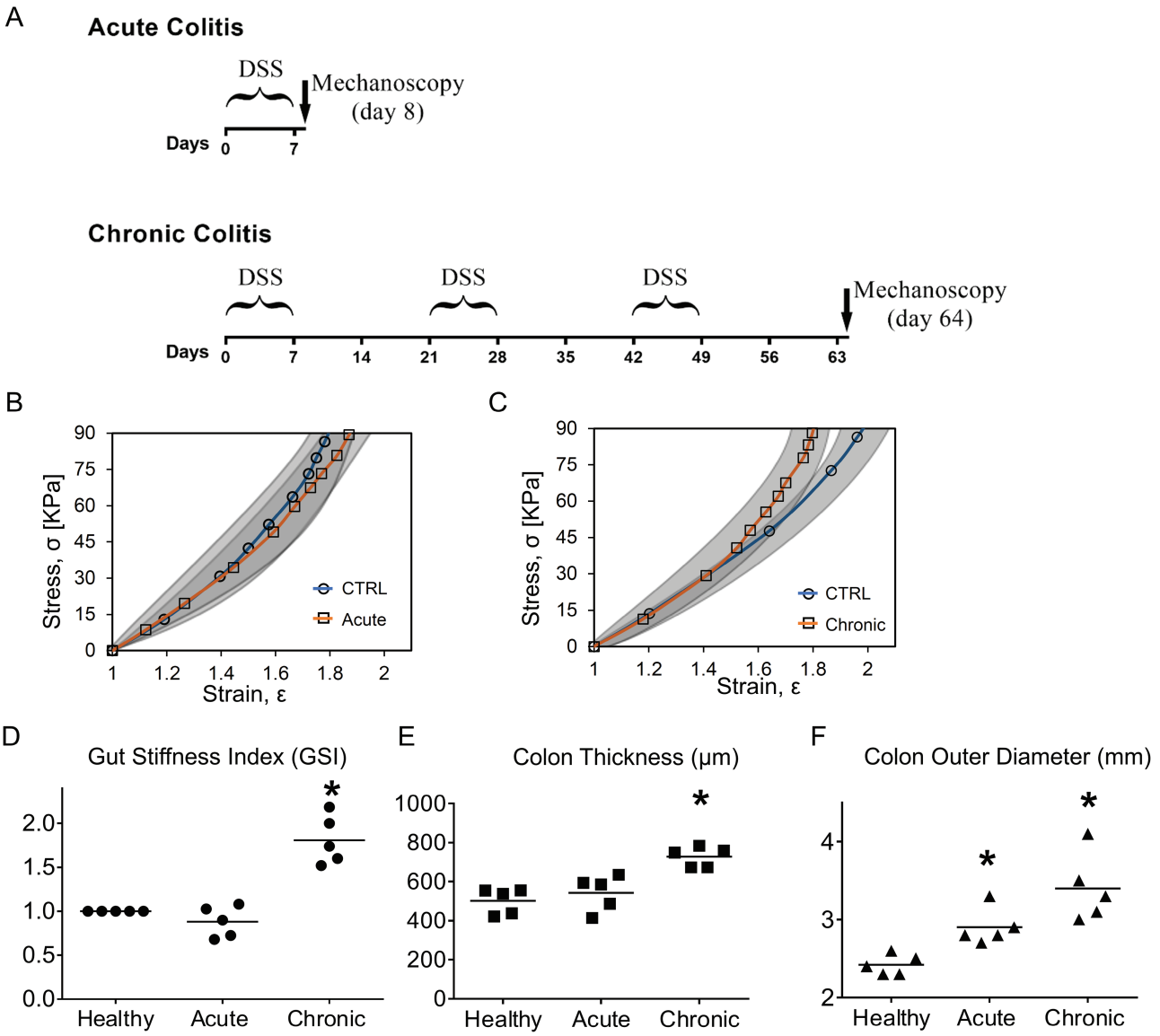


**Figure 2.** Gut diameter and gut stiffness index (GSI) for potential inflammation diagnosis. A, Illustration for the acute colitis model and the chronic colitis model. B, The stress-strain responses acquired from the deflation phase of colon show no significant difference between healthy group and acute colitis group. Gray areas show standard deviation. C, Beyond the critical strain at a level of 1.5, chronic colitis group shows significant colon stiffening compared with the healthy group. D, GSI is defined as the local slope of stress-strain curve at ε = 1.6 and normalized with respect to the healthy group. Gut stiffness index shows slight decreases for the acute group, but not significant decreases. However, GSI significantly increases about 1.8 times for chronic group. E, Compared with the healthy group, the chronic colitis colon significantly thickened 42%. F, Compared with the healthy group, the gut initial outer diameters increase significantly for both the acute and chronic groups. The chronic colitis group shows a greater increase ($n$ = 5, *V.S. healthy group, $P < .05$, Student $t$ test).

$$Corre\ (X, Y) = \frac{\sum (x - \bar{x})(y - \bar{y})}{\sqrt{\sum (x - \bar{x})^2 \sum (y - \bar{y})^2}} \qquad (5)$$

where $\bar{x}$ and $\bar{y}$ are, respectively, the average of the data $x$ and data $y$.

## RESULTS

### Mechanoscope

The mechanoscope for gut stiffness measurement comprises a control system, a pressure transducer, a water-filled balloon catheter, a syringe pump for the balloon inflation/deflation, and a diameter-detecting camera and gut diameter measurement module. (Figure 1A). The control system was developed based on LabVIEW (National Instruments, Austin, TX) with the following functions: (1) initiate communication with various system components (sensors and actuators); (2) actuate mechanical components (balloon inflation/deflation); (3) interact with operator via a graphic interface and real-time visualization of diameter measurement, user inputs, and errors, (4) automate repeatable tasks; and (5) tabulate data for further analysis (Figure 1A). The pressure and gut diameter were measured in real-time at a frequency of 1.9 Hz (114 times per minute).

To verify the safety of the gut stiffness measurement using the mechanoscope, after the measurement, ileum samples

from the test sites and the sites adjacent to them were collected for H&E staining (Figure 1B). No damage was detected in the samples from the test sites. The intact crypt-villus architecture and the continuous structure of the submucosa and muscle were maintained (Figure 1B).

In testing cycles, the gut outer diameter $D_{outer}$ was recorded in correspondence with total pressure $P_{total}$ in the balloon probe. Four phases were included in each testing cycle: balloon activation, inflation, deflation, and balloon residual. Figure 1C shows a representative inflation-deflation curve based on $P_{total}$ and $D_{outer}$ at a steady state.

The gut pressure ($P_{gut}$) was given by subtracting the balloon residual from $P_{total}$. In each test, the gut pressure ($P_{gut}$) and the corresponding outer diameter ($D_{outer}$) from the deflation curve were used for the gut stiffness measurement. We performed the mechanoscope *ex vivo* and *in vivo* for ileum samples from 20-week-old healthy mice (Figure 1D). The $P_{gut}$-$D_{outer}$ curves were acquired following 5 systematic preconditioning cycles. The *in vivo* and *ex vivo* results were in accordance with one another, verifying the repeatability and accuracy of the *in vivo* measurement using the mechanoscope. The *in vivo* setup was leveraged to record gut biomechanical response for the remaining experiments, which were then verified with the *ex vivo* setup.

Jejunum, ileum, and colon were used to examine whether the mechanoscope is capable of producing gut segment-specific biomechanical response. Each segment exhibited a distinct pressure-diameter curve when $P_{gut}$ changed from 0 to 40 mmHg (Figure 1E).

## Diagnosis Using the Mechanoscope for Colitis with both Acute and Chronic Phases in Mice

We applied the mechanoscope technology to diagnose dextran sulfate sodium (DSS)-induced acute and chronic colitis in mice. Acute colitis was induced by the administration of 3% DSS in drinking water for 1 week (Figure 2A). Chronic colitis was induced by 3 cycles of DSS administration. Each cycle included 1 week of 3% DSS (in drinking water) followed by 2 weeks of recovery (Figure 2A). Colon is the most affected tissue during DSS-induced colitis,[24–27] and colon biomechanical properties were measured using the mechanoscope. In the case of DSS-induced acute colitis, the stress-strain responses (Equation 2 and Equation 3) nearly overlapped with the healthy control group, suggesting there was no significant difference between the healthy and acute colitis groups in terms of gut stiffness (Figure 2B). However, in the case of chronic colitis, at strains $\varepsilon > 1.5$, the stress-strain response exhibited a more severe stiffening property (more abrupt slope of the stress-strain curve) compared with the healthy group (Figure 2C). This result provided a critical divergence point for distinguishing the stress-strain response in chronic colitis, which is at $\varepsilon = 1.5$. Beyond this point, the colon of the chronic colitis group became more stiffened than the healthy group. Thus, reaching the critical strain level is required for detecting the divergent biomechanical response in chronic colitis. The local slope of the stress-strain curves was used to define the gut stiffness index. Compared with the healthy control, when a GSI measured at $\varepsilon = 1.6$, it showed a nonsignificant change for the acute group, but significantly increased about 1.8 times for the chronic group (Figure 2D).

In addition, compared with the healthy group, the wall thickness of the chronic colitis colon increased by 42% (Figure 2E). The initial outer diameter $D_{outer,0}$ of the colon increased by 8.6% in the acute colitis group, whereas it increased by 19.3% in the chronic colitis group (Figure 2F). The thickening of the colon wall and the greater increase of the colon outer diameter observed in chronic colitis were accompanied by colon stiffening (Figures 2D-F).

Colon GSI was positively correlated with tissue fibrosis and severity of the DSS-induced colitis (Figure 3). In both acute and chronic models, disease induction was characterized by body weight loss, appearance of diarrhea, and visible fecal blood. The most recurring and severe symptoms were observed in the chronic model during the last DSS feeding cycle. Hematoxylin and eosin staining showed that compared with the healthy and acute colitis groups, the damage of colon mucosa and immune cell infiltration were most severe in the chronic groups (Figure 3A). As a sign of fibrosis, collagen deposition was much greater for the chronic colitis group compared with the acute colitis group, as shown on both Masson Trichrome staining (Figure 3B) and collagen-IV immunofluorescent staining (Figure 3C).

Based on the Masson Trichrome staining (Figure 3B) and the collagen immunofluorescent staining (Figure 3C), we calculated the fibrosis score (FS, Figure 4A), the normalized collagen deposition intensity (CDI, Figure 4B), and their correlation coefficient with GSI. For FS, "0" is scored for no fibrosis; and the higher the score, the more severe the fibrosis.[28] Although there were no significant differences between healthy colons and acute colitis colons with respect to the FS and CDI, they were both significantly greater in the chronic colitis colon (Figures 4A and B). Moreover, in the acute colitis colon, the correlation coefficients of the FS vs GSI and CDI vs GSI were –0.43 and –0.05, respectively, suggesting an absence of any correlations between the GSI and fibrosis severity (Figures 4C and D). For the chronic colitis colon, the correlation coefficients were 0.87 (for FS vs GSI, Figure 4E) and 0.92 (for CDI vs GSI, Figure 4F), indicating that the GSI score was strongly and positively correlated with fibrosis severity in the chronic colitis group. Therefore, the quantification of colon biomechanical score GSI using the mechanoscope can be potentially exploited for the diagnosis of gut fibrosis and determining the severity of the pathological damage induced by IBD.

## Diagnosis Using the Mechanoscope for Different Sites of Colon with Chronic Colitis

Using the mechanoscope, we diagnosed the nonuniform region-dependent development of chronic colitis in mouse colon. The biomechanical response of the proximal colon and the distal colon were measured (Figure 5A). After the measurement, the tissues from the same corresponding sites were collected for histology analysis (Figure 5B). The *in situ in vivo* stress-strain responses showed that compared with the proximal colon in the same mice with chronic colitis, stiffening (slope of the stress-strain curves) was more severe in the distal colon (Figure 5A). Gut stiffness index at $\varepsilon = 1.6$ increased by 19% in the distal colon compared with the proximal colon (Figure 5B). Correspondingly, compared with the proximal colon, the collagen deposition and the mucosa damage in the distal colon were more severe (Figures 5C and 5D). The correlation coefficient of CDI vs GSI across the proximal and distal colon is 0.90 (Figure 5E), suggesting the increase of GSI is strongly and positively

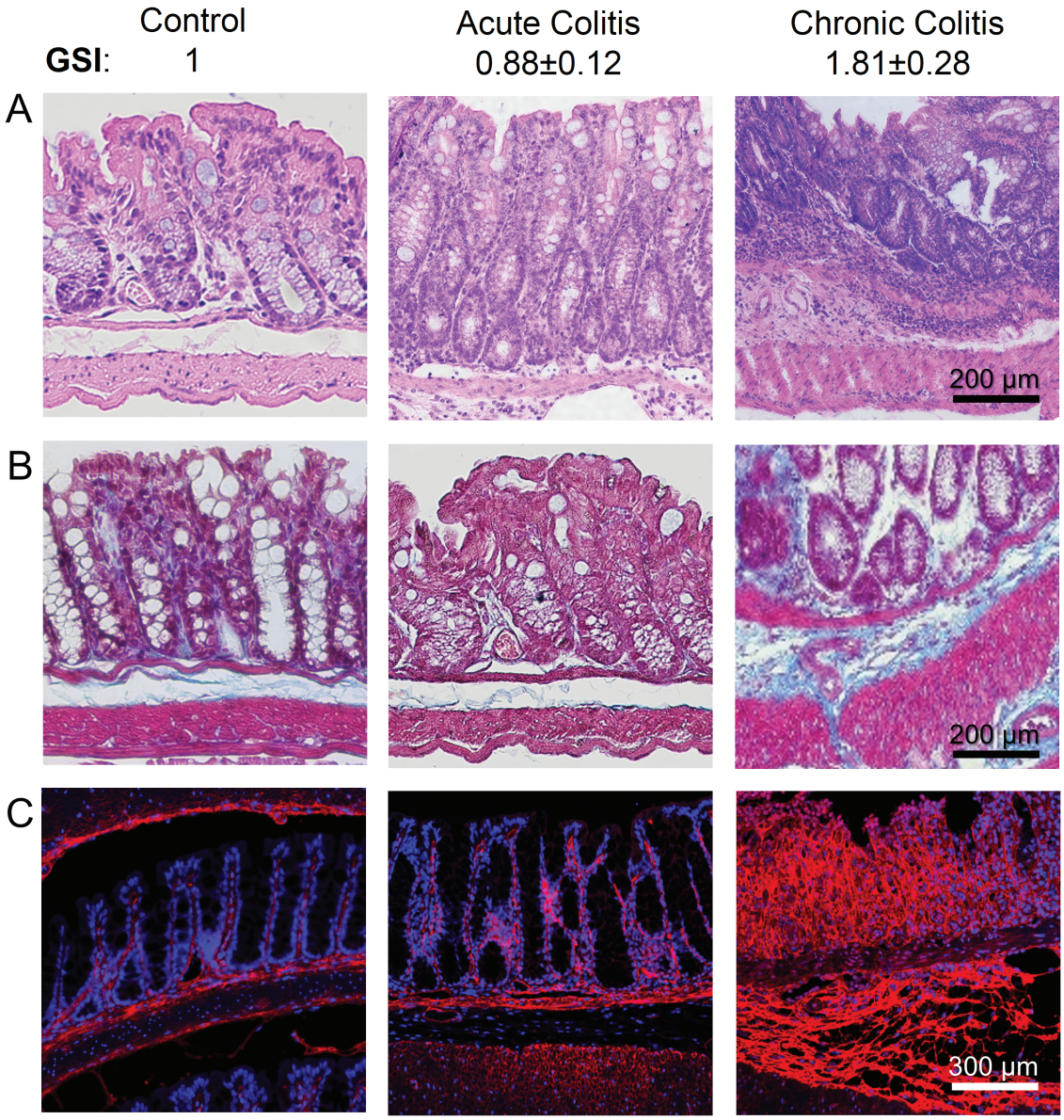


**Figure 3.** Gut stiffness index predicts the mouse colon fibrosis in chronic colitis. A, H&E staining, (B) Masson trichrome staining, and (C) collagen IV immunofluorescent staining from the healthy group, acute colitis group, and chronic colitis group, respectively. Compared with the healthy group and the acute colitis group, the GSI score is greater in the chronic colitis group. Correspondingly, the epithelial deterioration, collagen deposition, and tissue thickening are most severe in the chronic colitis group ($n = 5$).

correlated with the increase of fibrosis severity in the distal colon.

## DISCUSSION

Unlike previous methods characterizing biomechanical response of gut *in vitro* or *ex vivo*, we invented a novel strategy for measuring gut stiffness *in vivo*, called mechanoscopy. Using mechanoscopy, we can quantify gut stress-strain curves and score gut stiffness via the GSI, which is based on the slope of the stress-strain curves. When comparing acute colitis with chronic colitis or when comparing different regions of colon in chronic colitis, we showed that the higher the GSI, the greater the extent of gut fibrosis, the more severe the colon mucosal damage, and the more excessive the infiltrated immune cells. Based on these positive correlations between GSI and IBD severity, GSI and mechanoscopy could potentially be applied in IBD diagnosis. In addition, we demonstrated that the operation of mechanoscopy occurs under physiological loading conditions without inducing any tissue damage.

Using the DSS-induced colitis mouse model, we observed that the stress-strain response significantly diverged towards higher stiffness in the case of chronic colitis compared with healthy control. Further, the magnitude of the strain had to exceed a critical value ($\varepsilon = 1.5$) to identify the divergence. Prior to reaching this strain level, the differentiation of the biomechanical response was not significant between the healthy control and chronic colitis model. This could be explained if one envisions that beyond the critical strain, the fibrotic collagen switches configuration from an undulated state to a straight and tension-loaded state, thus contributing to stiffening at high strain levels.[15,29–31] These results suggest

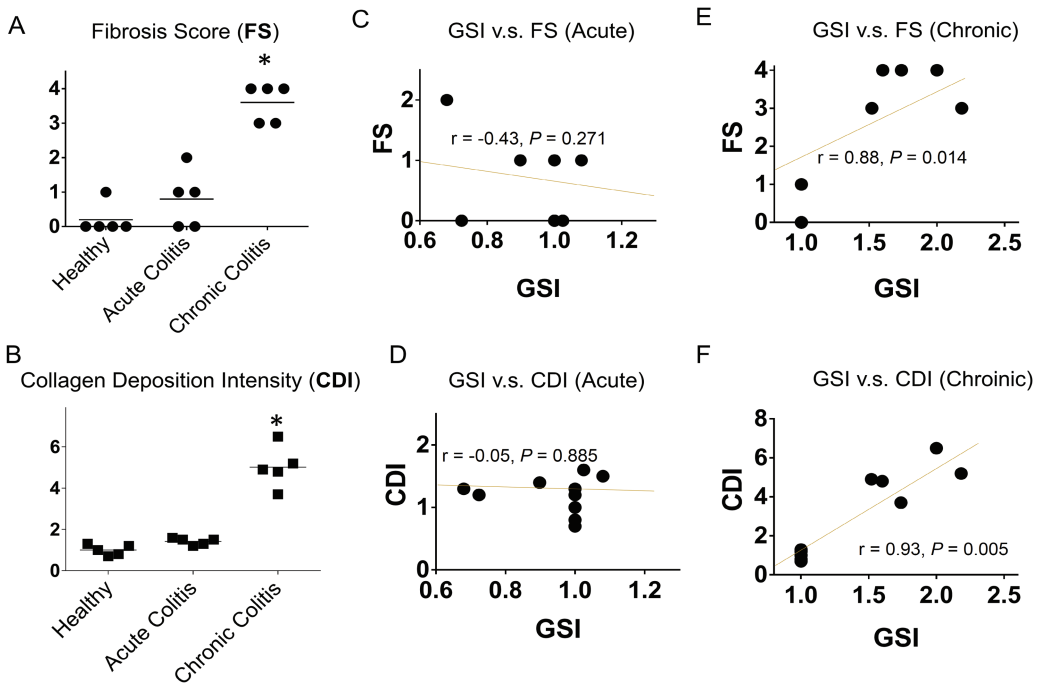


**Figure 4.** Gut stiffness index is positively correlated with the fibrosis score (FS) and collagen IV deposition intensity (CDI) in the chronic colitis colon. Quantification of FS (A) and CDI (B), correlation coefficients for GSI vs FS (C) and GSI vs CDI (D) of acute colitis colon, correlation coefficients for GSI vs FS (E) and GSI vs CDI (F) of chronic colitis colon. Correlation coefficient "1" suggests perfect positive correlation; "0" for no correlation; and "−1" for perfect negative correlation ($n$ = 5, *V.S. healthy group, $P < .05$, Student $t$ test).

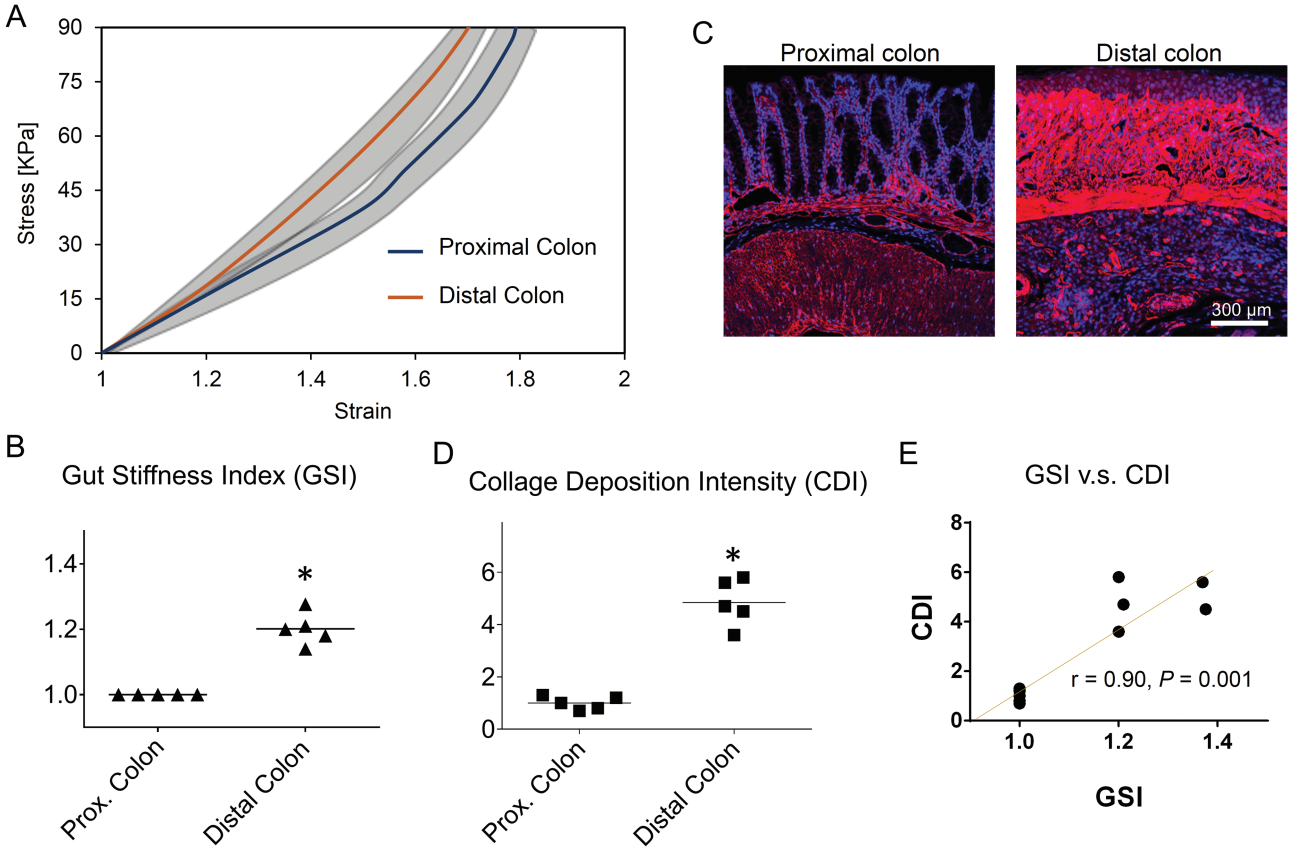


**Figure 5.** Gut stiffness index predicts the region-dependent fibrosis and severity of chronic colitis in mouse colon. A, The stress-strain responses showed that the stiffening of the colon was more severe in the distal region than in the proximal region. Gray areas show standard deviation. Gut stiffness index based on the slope of the stress-strain curves at ε=1.6 is normalized with respect to the proximal group. B, The GSI is increased by 19% in the distal colon compared with the proximal colon. C, The IF staining of collagen IV showed more excessive collagen deposition and more severe damage of the colon mucosa in the distal colon. D, The normalized CDI was greater in distal colon compared with the proximal colon. E, The correlation coefficient of GSI vs CDI across the proximal colon and the distal colon is 0.90 ($n$ = 5, *V.S. healthy group, $P < .05$, Student $t$ test).

that stiffening of the pathological fibrotic gut can be detected only when it surpasses the critical strain threshold ($\varepsilon = 1.5$).

Although no significant difference was detected in the GSI of acute colitis vs healthy tissue, there was a mild increase in the outer diameter of the colon in the acute colitis condition. In chronic colitis, the GSI, colon wall thickness, and colon outer diameter were all significantly increased. Thus, we propose two variables could be used to detect colitis, gut outer diameter (geometric variable), and GSI (biomechanical response variable). An increase of only the gut outer diameter suggests inflammation without gut stiffening, whereas an increase of both the outer diameter and GSI suggests more severe inflammation with gut stiffening. Taken together, these findings support mechanoscopy as a promising avenue for the translational application of gut diameter and stiffness measurement in IBD diagnosis.

## Funding

This work was supported by funding from National Institutes of Health K01DK103947 and Polsky family fund (to N.S.).

## Conflicts of Interest

The authors declare no conflict of interest.

## References

1. Stewart DC, Berrie D, Li J, et al. Quantitative assessment of intestinal stiffness and associations with fibrosis in human inflammatory bowel disease. *PLoS One*. 2018;13(7):e02003771–e02003716.
2. Zhao J, Liao D, Wilkens R, Krogh K, Glerup H, Gregersen H. Bowel stiffness associated with histopathologic scoring of stenosis in patients with Crohn's disease. *Acta Biomater*. 2021;130:332–342.
3. Venu VKP, Alston L, Iftinca M, et al. Nr4A1 modulates inflammation-associated intestinal fibrosis and dampens fibrogenic signaling in myofibroblasts. 2021;321(3):G297–G297.
4. Johnson LA, Rodansky ES, Sauder KL, et al. Matrix stiffness corresponding to strictured bowel induces a fibrogenic response in human colonic fibroblasts. *Inflamm Bowel Dis*. 2013;19(5):891–903.
5. Gabbiadini R, Zacharopoulou E, Furfaro F, et al. Application of ultrasound elastography for assessing intestinal fibrosis in inflammatory bowel disease: fiction or reality? *Curr Drug Targets*. 2021;22(3):347–355.
6. Kobayashi H, Enomoto A, Woods S, Burt AD, Takahashi M, Worthley DL. Cancer-associated fibroblasts in gastrointestinal cancer. *Nat Rev Gastroenterol Hepatol*. 2019;16(5):282–295.
7. Ciasca G, Papi M, Minelli E, Palmieri V, De Spirito M. Changes in cellular mechanical properties during onset or progression of colorectal cancer. *World J Gastroenterol*. 2016;22(32):7203.
8. Stidham RW, Xu J, Johnson LA, et al. Ultrasound elasticity imaging for detecting intestinal fibrosis and inflammation in rats and humans with Crohn's disease. *Gastroenterology*. 2011;141(3):819–826.e1.
9. Prim DA, Potts JD, Eberth JF. Pulsatile perfusion bioreactor for biomimetic vascular impedances. *J Med Device*. 2018;12(4):041002.
10. Tower TT, Neidert MR, Tranquillo RT. Fiber alignment imaging during mechanical testing of soft tissues. *Ann Biomed Eng*. 2002;30:1221–1233.
11. Carew EO, Barber JE, Vesely I. Role of preconditioning and recovery time in repeated testing of aortic valve tissues: validation through quasilinear viscoelastic theory. *Ann Biomed Eng*. 2000;28:1093–1100.
12. Miller KS, Edelstein L, Connizzo BK, Soslowsky LJ. Effect of preconditioning and stress relaxation on local collagen fiber re-alignment: inhomogeneous properties of rat supraspinatus tendon. *J Biomech Eng*. 2012;134(3):31007.
13. Ebrahimi M, Mohammadi A, Ristaniemi A, Stenroth L, Korhonen RK. The effect of different preconditioning protocols on repeatability of bovine ACL stress-relaxation response in tension. *J Mech Behav Biomed Mater*. 2019;90:493–501.
14. Azar D, Ohadi D, Rachev A, Eberth JF, Uline MJ, Shazly T. Mechanical and geometrical determinants of wall stress in abdominal aortic aneurysms: a computational study. *PLoS One*. 2018;13(2):e0192032.
15. Rachev A, Shazly T. A structure-based constitutive model of arterial tissue considering individual natural configurations of elastin and collagen. *J Mech Behav Biomed Mater*. 2019;90:61–72.
16. Ito R, Kita M, Ya MS, et al. Involvement of IL-17A in the pathogenesis of DSS-induced colitis in mice. *Biochem Biophys Res Commun*. 2008;377(1):12–16.
17. Gaudio E, Taddei G, Vetuschi A, et al. Dextran Sulfate Sodium (DSS) colitis in rats clinical, structural, and ultrastructural aspects. *Dig Dis Sci*. 1999;44(7):1458–1475.
18. Kim CJ, Kovacs-Nolan JA, Yang C, Archbold T, Fan MZ, Mine Y. L-Tryptophan exhibits therapeutic function in a porcine model of dextran sodium sulfate (DSS)-induced colitis. *J Nutr Biochem*. 2010;21(6):468–475.
19. Okayasu I, Hatakeyama S, Yamada M, Ohkusa T, Inagaki Y, Nakaya R. A novel method in the induction of reliable experimental acute and chronic ulcerative colitis in mice. *Gastroenterology*. 1990;98(3):694–702.
20. Kianmehr P, Azarbayjani MA, Peeri M, Farzanegi P. Synergic effects of exercise training and octopamine on peroxisome proliferator-activated receptor-gamma coactivator -1a and uncoupling protein 1 mRNA in heart tissue of rat treated with deep frying oil. *Biochem Biophys Rep*. 2020;22:100735.
21. Torenbeek R, Hermsen MAJA, Meijer GA, Baak JA, Meijer CJLM. Analysis by comparative genomic hybridization of epithelial and spindle cell components in sarcomatoid carcinoma and carcinosarcoma: histogenetic aspects. *J Pathol*. 1999;189(3):338–343.
22. Manetti M, Rosa I, Messerini L, Ibba-Manneschi L. Telocytes are reduced during fibrotic remodelling of the colonic wall in ulcerative colitis. *J Cell Mol Med*. 2015;19(1):62–73.
23. Xu X, Lin S, Yang Y, et al. Histological and ultrastructural changes of the colon in dextran sodium sulfate-induced mouse colitis. *Exp Ther Med*. 2020;20(3):1987–1994.
24. Carlsson AH, Yakymenko O, Olivier I, et al. Faecalibacterium prausnitzii supernatant improves intestinal barrier function in mice DSS colitis. *Scand J Gastroenterol*. 2013;48(10):1136–1144.
25. Azuma YT, Nishiyama K, Matsuo Y, et al. PPARα contributes to colonic protection in mice with DSS-induced colitis. *Int Immunopharmacol*. 2010;10(10):1261–1267.
26. Laroui H Ingersoll SA, Liu HC, et al. Dextran Sodium Sulfate (DSS) Induces colitis in mice by forming nano-lipocomplexes with medium-chain-length fatty acids in the colon. *PLoS One*. 2012;7(3):e32084.
27. Yao J, Wang J, Liu L, et al. Anti-oxidant effects of resveratrol on mice with DSS-induced ulcerative colitis. *Arch Med Res*. 2010;41(4):288–294.
28. Masseroli M, Caballero T, O'Valle F, Del Moral RMG, Pérez-Milena A, Del Moral RG. Automatic quantification of liver fibrosis: design and validation of a new image analysis method: comparison with semi-quantitative indexes of fibrosis. *J Hepatol*. 2000;32(3):453–464.
29. Gasser TC, Gallinetti S, Xing X, Forsell C, Swedenborg J, Roy J. Spatial orientation of collagen fibers in the abdominal aortic aneurysm's wall and its relation to wall mechanics. *Acta Biomater*. 2012;8(8):3091–3103.
30. Komuro T. The lattice arrangement of the collagen fibres in the submucosa of the rat small intestine: scanning electron microscopy. *Cell Tissue Res*. 1988;251:117–121.
31. Orberg J, Baer E, Hiltner A. Organization of collagen fibers in the intestine. *Connect Tissue Res*. 2009;11(4):285–297.